Available online at www.sciencedirect.com
SCIENCE DIRECT
International Journal of Heat and Mass Transfer 49 (2006) 2957–2964
International Journal of HEAT and MASS TRANSFER
www.elsevier.com/locate/ijhmt

# Tree-shaped flow structures with local junction losses

W. Wechsatol [a], S. Lorente [b], A. Bejan [c,*]

[a] Department of Mechanical Engineering, King Mongkut's University of Technology, Thonburi, Rasburana, Bangkok 10140, Thailand
[b] Laboratoire Matériaux et Durabilité des Constructions, Institut National des Sciences Appliquées, Département de Génie Civil, 135 Avenue de Rangueil, Toulouse 31077, France
[c] Department of Mechanical Engineering and Materials Science, Box 90300, Duke University, Durham, NC 27708-0300, USA

Received 11 July 2005; received in revised form 21 January 2006
Available online 17 April 2006

**Abstract**

This paper is a fundamental study of the effect of junction losses on the optimized geometry of tree-shaped flows. Several classes of flows are investigated systematically in a T-shaped construct with fixed internal and external size: laminar with non-negligible entrance and junction losses, and turbulent in tubes with smooth and rough walls. It is shown that in all cases junction losses have a sizeable effect on optimized geometry when $Sv^2 < 10$, where the svelteness $Sv$ is a global property of the entire flow system: $Sv =$ external length scale/internal length scale. The relationship between the global $Sv$ and the slenderness of individual channels is discussed. The study shows that, in general, the duct slenderness decreases as the tree architecture becomes finer and more complex. In conclusion, miniaturization pushes flow architectures not only toward the smaller, finer and more complex, but also toward the domain in which junction losses must be taken into account in the optimization of geometry.


*Keywords:* Tree-shaped; Dendritic; Constructal theory; Junction losses; Svelteness

## 1. Introduction

The drive towards flow structures with maximum density of heat transfer has generated a growing body of work on tree-shaped flow architectures [1,2]. Several studies of conduction [3–5] and convection [6–13] have shown that tree-shaped distribution and collection architectures offer better (more uniform) use of every elemental volume of the finite space that is available. The reason is that the tree is the flow architecture that provides the easiest (fastest, most direct) flow access between one point (source, or sink) and an infinity of points (curve, area, or volume).

The traditional design of compact and miniaturized flow architectures is based on a single length scale that is distributed uniformly through the available space, e.g., parallel microchannels of one size, and bundles of tubes of one size positioned in cross flow. Tree-shaped architectures depart from tradition in two important respects: (a) they possess multiple length scales that are arranged hierarchically, and (b) the length scales are distributed optimally (non-uniformly) through the constrained space. In the optimized architecture, there is one place for the trunk of the tree, and another for the canopy. There is an optimal subvolume (interstice) to be allocated to the smallest (finite size) branch. The non-uniformity and complexity of the tree structure are results of the optimization of architecture. They are not assumptions, and they are not objectives: optimized complexity must not be confused with maximized complexity.

Tree architectures for fluid flow have been analyzed and optimized based on the simplest model: Poiseuille flow in slender channels where the local pressure losses at the junctions are assumed to be negligible (e.g., Refs. [9] and [11]). On the other hand, simulations of flows through tree-shaped structures (e.g. Ref. [8]) have shown that local losses are present. Even if at low flow rates the channel

* Corresponding author. Tel.: +1 919 660 5309; fax: +1 919 660 8963.
*E-mail address:* dalford@duke.edu (A. Bejan).

0017-9310/$ - see front matter © 2006 Elsevier Ltd. All rights reserved.
doi:10.1016/j.ijheatmasstransfer.2006.01.047

**Nomenclature**

| | |
|---|---|
| $A$ | area, $m^2$ |
| $A_p$ | projected area of all the ducts, $m^2$ |
| $B$ | pressure drop number, Eq. (16) |
| $D$ | duct diameter or spacing, m |
| $f$ | friction factor, Eq. (7) |
| $f_T$ | junction loss factor |
| $k_s$ | roughness height, m |
| $K$ | junction loss coefficient |
| $L$ | duct length, m |
| $\dot{m}$ | mass flow rate, kg $s^{-1}$ |
| $\dot{m}'$ | mass flow rate per unit length, kg $s^{-1}$ $m^{-1}$ |
| $n_i$ | number of tubes of the same length |
| $N$ | number of ports on the rim |
| $p$ | number of pairing levels |
| $Q$ | volumetric flow rate, $m^3$ $s^{-1}$ |
| $R$ | external length scale, m |
| $R_f$ | overall flow resistance, Eq. (23) |
| $Re$ | Reynolds number, Eq. (17) |
| $Sv$ | svelteness, Eq. (3) |
| $u$, $v$ | velocity components, m $s^{-1}$ |
| $V$ | total duct volume, $m^3$ |
| $U$ | mean velocity, m $s^{-1}$ |
| $x$, $y$ | Cartesian coordinates, m |

*Greek symbols*

| | |
|---|---|
| $\Delta P$ | pressure difference, Pa |
| $\mu$ | viscosity |
| $\nu$ | kinematic viscosity, $m^2$ $s^{-1}$ |
| $\rho$ | density, kg $m^{-3}$ |

*Superscripts*

| | |
|---|---|
| $\hat{(\ )}$ | dimensionless, Eq. (1) |
| $\tilde{(\ )}$ | dimensionless, Eqs. (8), (14) and (15) |

with Poiseuille flow has negligible local losses, at sufficiently high flow rates the channel may be dominated by local losses while the flow regime is still laminar.

In this paper we investigate the effect that local losses have on the optimized architecture of a tree-shaped flow. This is a new question that goes beyond the traditional evaluation of the relative importance of pressure losses (distributed vs. local) in a channel or duct. Here we ask under what conditions and in what ways do the local losses affect the optimized tree geometry. Related to this is the question of determining in clear and general terms the domain of validity of the tree flow architectures that have been optimized based on the assumption that local losses are negligible.

## 2. Svelteness vs. slenderness

The answer to the preceding question is more challenging and interesting than the mere evaluation of the relative size of local losses as a function of the flow regime. The answer depends on the architecture itself, and it becomes more important as the architecture becomes more complex. To see why, consider the class of tree-shaped architectures that connect a circle with its center (Fig. 1). The total liquid flow rate between the center and the rim is $\dot{m}$. The circle radius ($R$) and the total volume of all the ducts ($V$) are fixed. The overall pressure difference ($\Delta P$) between the center and the rim depends on the tree architecture, which is described by the tube lengths ($L_i$), the numbers of tubes of the same length ($n_i$), the tube diameters ($D_i$), and the number of tube pairing levels ($p$), where $i$ increases from the center toward the rim ($i = 0, 1, \ldots, p$).

In Ref. [11] we have optimized trees of the point-to-circle class in the wide range represented by $0 \leqslant p \leqslant 5$ and $3 \leqslant N \leqslant 400$, where $N$ is the number of ports on the rim ($N = n_p$). In this paper we have extended this range by optimizing trees with six and seven levels of pairing: two examples of this new work are now illustrated in Fig. 1. In all these optimized flow structures we have assumed Poiseuille flow with negligible junction losses, and we have minimized the overall flow resistance $\Delta P/\dot{m}$ by morphing the architecture through all its possible flow configurations. In this way we obtained the optimal tube lengths and their layout (e.g., Fig. 1), and the optimal relative tube diameters, which follow the Hess–Murray law: $D_{i+1}/D_i = 2^{-1/3}$.

Because local losses are expected to be negligible in the limit where all the ducts are sufficiently slender, in Fig. 2 we report the slenderness of the ducts of all the optimized trees with three tubes in the center ($n_0 = 3$). The slenderness of one tube ($L_i/D_i$) depends on two items: its position in the tree structure, and the global constraints, namely the external size $R$, and the total tube volume $V$. These two items are separated and put on display in Fig. 2 by plotting the slenderness $L_i/D_i$ ratio in dimensionless terms,

$$\hat{L}_i = \frac{L_i}{R}, \quad \hat{D}_i = \frac{D_i}{V^{1/3}} \tag{1}$$

such that

$$\frac{L_i}{D_i} = Sv\frac{\hat{L}_i}{\hat{D}_i} \tag{2}$$

where the *svelteness* $Sv$ is a global parameter [14] that is fixed by the size constraints ($R, V$):

$$Sv = \frac{\text{external length scale}}{\text{internal length scale}} = \frac{R}{V^{1/3}} \tag{3}$$

Unlike the duct slenderness $L_i/D_i$, the svelteness $Sv$ is a parameter that describes the whole architecture, not its components. Qualitatively, the $Sv$ number defined in Eq.

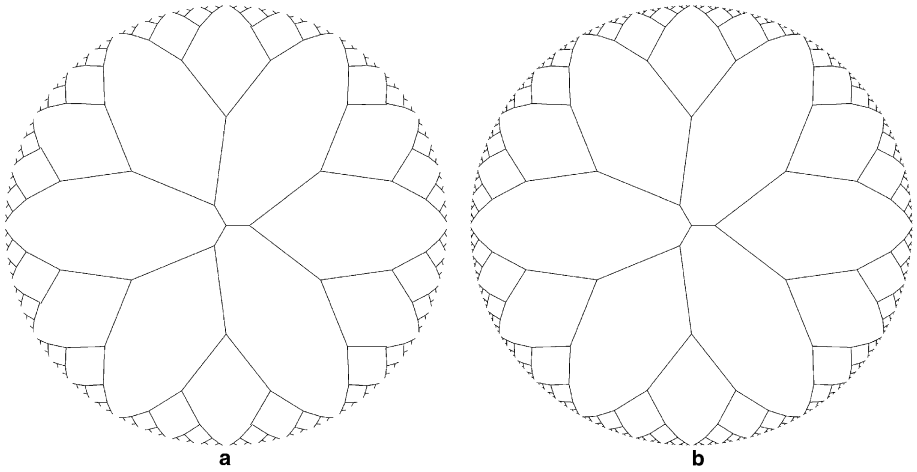


Fig. 1. Optimal tree-shaped flow architecture connecting the center of a disc with many points distributed uniformly on the rim: (a) $n_0 = 3$, $p = 6$, $N = 192$ and (b) $n_0 = 3$, $p = 7$, $N = 384$.

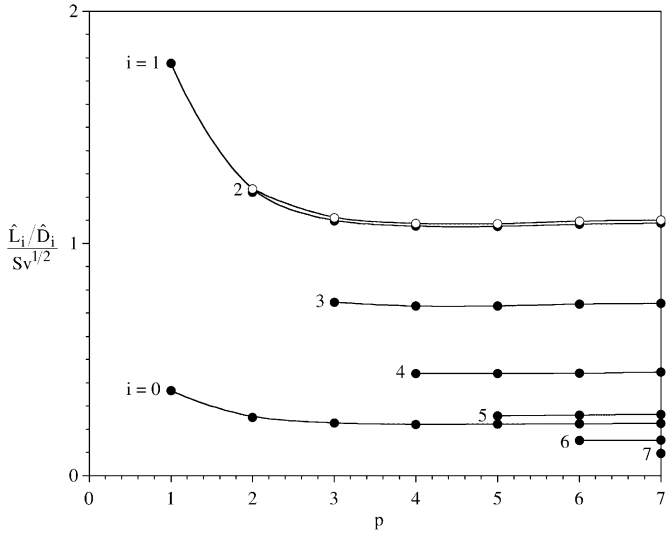


Fig. 2. The slenderness of the tubes of optimized point-circle trees with $n_0 = 3$.

(3) is related to the slenderness of the ducts: if the appropriate scale for $L_i$ is $R$ (not $V^{1/3}$, as in Eq. (3)), then $V$ scales as $D_i^2 R$, and the slenderness ratio $L_i/D_i$ scales as $Sv^{3/2}$. Svelte tree architectures have slender ducts.

Fig. 2 refers to the slenderness ratio $L_i/D_i$ of any tube in tree structure such as Fig. 1. The abscissa of Fig. 2 indicates the number of pairing or bifurcation levels of the structure. The number $i$ indicates the position of the tube relative to the disc center. For example, $i = 0$ refers to tubes that touch the center, and $i = p$ to tubes that touch the rim. Reading Fig. 2 in the vertical cut made at $p = 3$, we see that the structure has four types of tubes: $i = 0$, 1, 2 and 3.

Fig. 2 shows that the slenderness of every duct ($L_i/D_i$) increases in proportion with the specified global value $Sv$. The less expected message of Fig. 2 is that, in general, tube slenderness *decreases* as the tree architecture becomes more complex. Looking into the future, where miniaturization pushes flow architectures toward optimized trees that are increasingly more complex because their smallest elements become smaller and more numerous, we see that the optimized channels are destined to become less slender, and the model on which their optimization was based becomes suspect. This is why the effect of local losses must be taken into account in the generation of optimal tree architectures. In the work described in this paper, we examine this effect by focusing on the simplest element of a tree-shaped structure, namely, the junction between two small ducts and a larger duct.

## 3. Laminar flow

Consider the optimization of the two-dimensional flow configuration shown in Fig. 3a. One channel of width $D_1$ communicates with two channels of width $D_2$. The entire T-shaped construct occupies a rectangular territory of fixed size

$$2L_1L_2 = A, \quad \text{constant} \tag{4}$$

The shape of the territory ($L_2/L_1$) is not specified. The total projected area of all the channels is fixed,

$$D_1(L_1 - D_2) + 2D_2L_2 = A_p, \quad \text{constant} \tag{5}$$

The relative size of the channels ($D_2/D_1$) varies. Constraint (4) shows that the channel lengths $L_i$ ($i = 1, 2$) scale as $A^{1/2}$, while constraint (5) sets the scale of $D_i$ at $A_p/A^{1/2}$. This leads to the conclusion that the slenderness of the channels $L_i/D_i$ is of order $A/A_p$, and that the dimensionless constraint obtained by combining constraints (4) and (5) is the svelteness, cf. Eq. (3),

$$Sv = \frac{A^{1/2}}{A_p^{1/2}} \tag{6}$$

In two-dimensional flow, the svelteness squared is the inverse of the area fraction occupied by all the channels on the fixed territory ($A_p/A$).

The objective is to select the configuration that allows a fluid to flow with a minimal resistance $\Delta P/\dot{m}'$ through the construct, where $\Delta P$ is the overall pressure difference, and $\dot{m}'$ (kg s$^{-1}$ m$^{-1}$) is the mass flow rate through the $L_1$ channel, per unit length in the direction perpendicular to Fig. 3. The configuration has two degrees of freedom, $L_2/L_1$ and $D_2/D_1$. The fluid properties are constant. The optimization can be executed analytically in the limit of sufficiently svelte channels ($Sv \gg 1$), such that the Poiseuille regime prevails in all the channels, the local pressure losses are negligible, and the same solution holds for both flow directions, splitting flow and merging flow. We use this limiting solution as reference for the optimized configurations that we determine numerically for lower values of $Sv$. By calculating the total pressure drop along the $L_1$ and $L_2$ channels in series, one can show that the overall flow resistance is

$$\frac{\Delta P}{\dot{m}'} = 12\frac{\nu Sv^6}{A} f \tag{7}$$

where

$$f = \left[(\tilde{L}_1 - \tilde{D}_2) + \frac{1}{4\tilde{L}_1}\left(\frac{D_1}{D_2}\right)^3\right]\left((\tilde{L}_1 - \tilde{D}_2) + \frac{D_2/D_1}{\tilde{L}_1}\right)^3 \tag{8}$$

with $\tilde{L}_1 = L_1/A^{1/2}$ and $\tilde{D}_2 = D_2/A^{1/2}$. In the limit $Sv \gg 1$, the length $L_i$ is much larger than the channel width $D_i$. Therefore Eq. (8) reduces to

$$f = \left[\tilde{L}_1 + \frac{1}{4\tilde{L}_1}\left(\frac{D_1}{D_2}\right)^3\right]\left(\tilde{L}_1 + \frac{D_2/D_1}{\tilde{L}_1}\right)^3 \tag{9}$$

To minimize $\Delta P/\dot{m}'$ subject to fixed $A$ and $Sv$ is the same as minimizing $f$ with respect to $\tilde{L}_1$ and $D_2/D_1$. This operation pinpoints the optimal configuration, which is characterized by

$$\left(\frac{L_2}{L_1}\right)_{\text{opt}} = \left(\frac{D_2}{D_1}\right)_{\text{opt}} = 2^{-1/2}, \quad f_{\min} = 8 \tag{10}$$

When $Sv$ is not large, junction losses play a role and so does the direction of the flow through the T construct. Consider first the splitting flow shown in Fig. 3a. The flow is governed by the mass and momentum conservation equations

$$\frac{\partial \tilde{u}}{\partial \tilde{x}} + \frac{\partial \tilde{v}}{\partial \tilde{y}} = 0 \tag{11}$$

$$\tilde{u}\frac{\partial \tilde{u}}{\partial \tilde{x}} + \tilde{v}\frac{\partial \tilde{u}}{\partial \tilde{y}} = -\frac{1}{B}\frac{\partial \tilde{P}}{\partial \tilde{x}} + \frac{1}{B}\left(\frac{\partial^2 \tilde{u}}{\partial \tilde{x}^2} + \frac{\partial^2 \tilde{u}}{\partial \tilde{y}^2}\right) \tag{12}$$

$$\tilde{u}\frac{\partial \tilde{v}}{\partial \tilde{x}} + \tilde{v}\frac{\partial \tilde{v}}{\partial \tilde{y}} = -\frac{1}{B}\frac{\partial \tilde{P}}{\partial \tilde{y}} + \frac{1}{B}\left(\frac{\partial^2 \tilde{v}}{\partial \tilde{x}^2} + \frac{\partial^2 \tilde{v}}{\partial \tilde{y}^2}\right) \tag{13}$$

The numerical simulations were conducted in dimensionless terms by using the dimensionless variables

$$(\tilde{x}, \tilde{y}, \tilde{D}_1, \tilde{D}_2, \tilde{L}_1, \tilde{L}_2) = (x, y, D_1, D_2, L_1, L_2)/A^{1/2} \tag{14}$$

$$(\tilde{u}, \tilde{v}) = (u, v)\frac{\mu}{A^{1/2}\Delta P} \quad \tilde{P} = \frac{P - P_0}{\Delta P} \tag{15}$$

where $\tilde{u}$ and $\tilde{v}$ are the velocity components in the $\tilde{x}$ and $\tilde{y}$ directions, while $\Delta P = P_1 - P_0$. The pressure is assumed constant and uniform ($P = \Delta P$) over the inlet plane of the $L_1$ channel. The lowest pressure ($P = 0$) is maintained constant and uniform over the outlet planes of the $L_2$ chan-

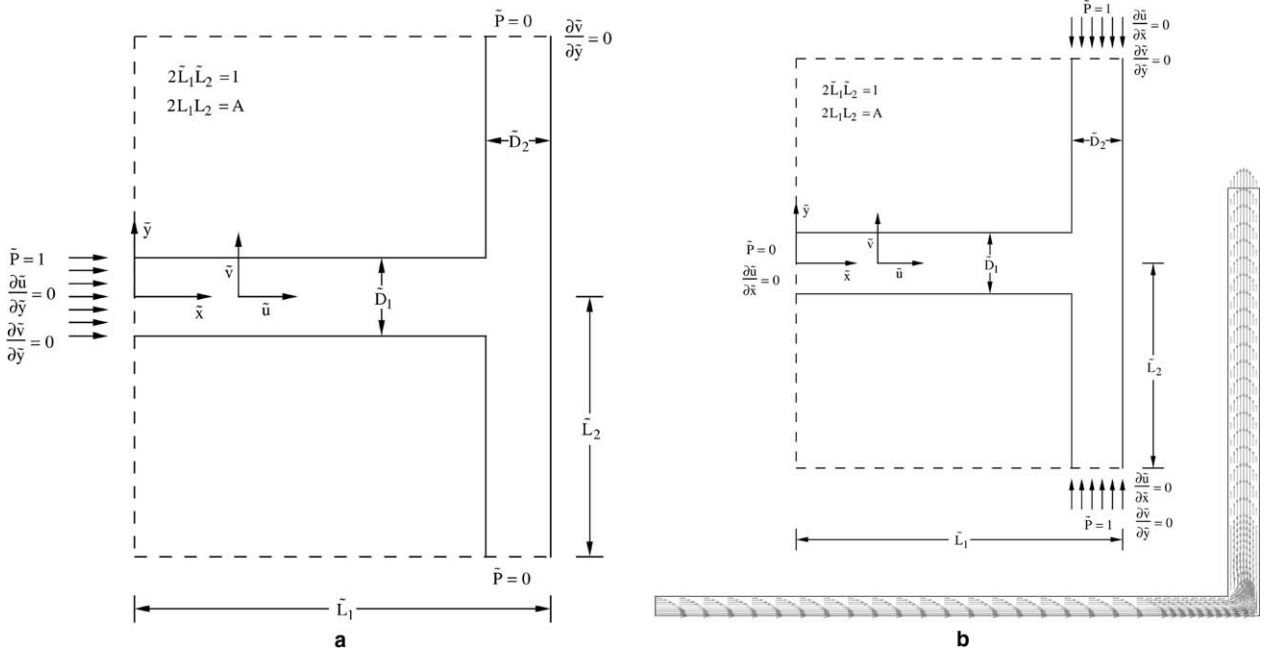


Fig. 3. Two-dimensional T-shaped constructs with (a) splitting flow, and (b) merging flow. Patterns of velocity profile when $B = 100$ and $Sv = 3.16$ (or $A_p/A = 0.1$) are shown at the bottom.

nels. The channel surfaces are impermeable with no slip. The dimensionless pressure drop number $B$ is defined by

$$B = \frac{\Delta P A}{\mu v} \tag{16}$$

We solved these equations and simulated the flow field by using a finite elements package [15]. To validate the accuracy of the code we reproduced the flow simulations presented recently by Aydin et al. [16], who applied the boundary element method to simulate laminar flow in a T channel. Their velocity profiles agree with the results obtained by us numerically. Furthermore, in the limit that $Sv^2 \gg 1$, the flow resistance $f$ obtained numerically in this study approaches the analytical result, Eq. (10), as we show later in Fig. 6.

The relations between the pressure drop number $B$ and the Reynolds numbers for the two channels are

$$Re_1 = \frac{2D_1U_1}{v} = 2\tilde{U}_1\tilde{D}_1B \quad \text{and} \quad Re_2 = \frac{2D_2U_2}{v} = 2\tilde{U}_2\tilde{D}_2B \tag{17}$$

where $U_1$ and $U_2$ are the respective mean longitudinal velocities, and $2D_1$ and $2D_2$ are the hydraulic diameters. The flow conditions at the inlet and the two outlets are indicated in Fig. 3a for splitting flow, and Fig. 3b for merging flow. The inlet flow is assumed uniform, while its velocity is a calculated result, because it depends on the assumed flow geometry. At the two outlets we imposed $\partial\tilde{v}/\partial\tilde{y} = 0$, as an assumption of full development in the vicinity of the outlets.

The numerical code was based on quadrilateral elements with four nodes, which were distributed non-uniformly to cover the flow domain. The grid fineness was changed stepwise, by decreasing the grid spaces to half of their original values. These changes stopped, and the grid was considered fine enough when the relative changes in the total flow rate through the structure were less than $10^{-3}\%$. The bottom of Fig. 3 shows examples of the velocity field in a case where local losses are not negligible.

The optimization procedure consisted of holding $B$ and $Sv$ fixed, and simulating the flow in a large number of configurations, one differing slightly from the next. Because the overall pressure difference was fixed ($B$), the search was for the configuration ($L_2/L_1$, $D_2/D_1$) with the largest flow rate. The results are reported in Figs. 4–6. The results approach the limiting solution for negligible junction losses, Eq. (10).

The solid curves in Fig. 4 show that $(D_2/D_1)_{opt}$ approaches the limit of Eq. (10) as the svelteness of the structure increases. The optimal diameter ratio of the merging flow behaves in the same way. The figure shows that the effect of junction losses is negligible when $Sv^2$ is larger than 10. Note that in case of merging flow with high pressure drop number $B$ the junction losses have no effect on the optimal diameter ratio.

Fig. 5 shows that the optimal aspect ratio of the covered area $(L_2/L_1)_{opt}$ is insensitive to either the svelteness or the pressure drop number $B$. Taken together, Figs. 4 and 5 document the effect of flow direction on optimal

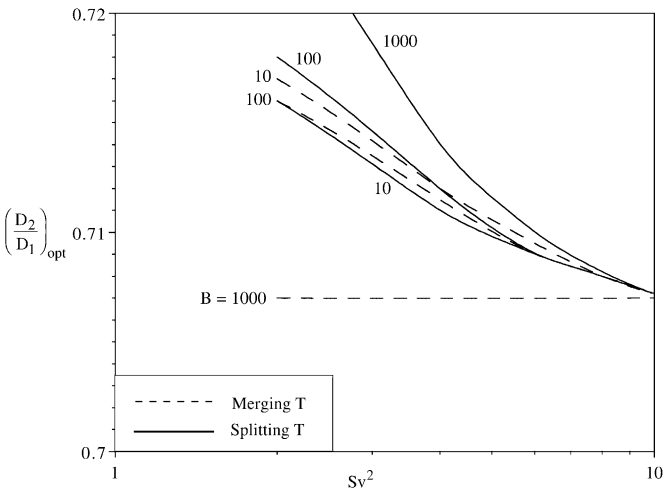


Fig. 4. The optimal diameter ratio for T-shaped constructs with laminar flow, Fig. 3.

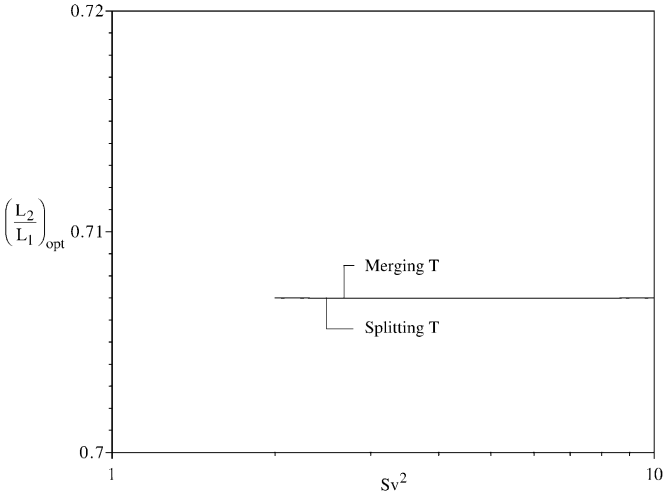


Fig. 5. The optimal ratio of channel lengths for T-shaped constructs with laminar flow, Fig. 3.

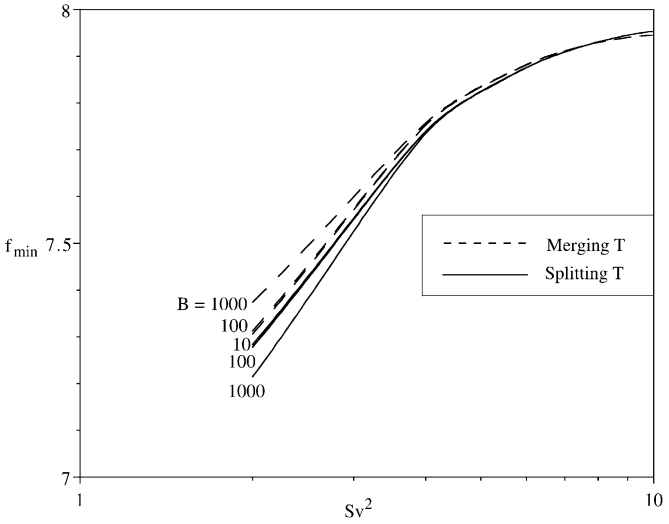


Fig. 6. The minimal overall flow resistance for T-shaped constructs with laminar flow, Fig. 3.

configuration. The flow direction plays a role when the junction pressure loss is not negligible. The same conclusion is reached in Fig. 6, by comparing the limiting ($f_{\min} = 8$, Eq. (10)) with the overall flow resistance minimized numerically. The flow resistance approaches the limit value as $Sv$ increases.

## 4. Turbulent flow through smooth ducts

The effect of junction losses on the optimal geometry when the flow is turbulent can be studied based on the data provided by Idelchik [17] for T-shaped junctions of round pipes. Consider again Fig. 3, and assume that the rectangular $A$ area houses one round pipe of length $L_1$ and internal diameter $D_1$, and two round pipes of length $L_2$ and internal diameter $D_2$. The overall pressure difference ($\Delta P$) is fixed. The total mass flow rate ($\dot{m}$) varies as the geometry of the T-shaped construct changes. We seek the configuration in which $\dot{m}$ is maximum. The external size constraint (4) continues to hold. The internal size constraint (5) is replaced by

$$V = \frac{\pi}{4}D_1^2(L_1 - D_2) + 2\frac{\pi}{4}D_2^2 L_2, \quad \text{constant} \tag{18}$$

For simplicity we assume that $D_2$ is much smaller than $L_1$, so that Eq. (18) reduces to

$$V = \frac{\pi}{4}D_1^2 L_1 + 2\frac{\pi}{4}D_2^2 L_2, \quad \text{constant} \tag{19}$$

The svelteness is defined in accordance with Eq. (3),

$$Sv = \frac{A^{1/2}}{V^{1/3}}, \quad \text{constant} \tag{20}$$

According to Ref. [17], the overall pressure drop is calculated as $\Delta P = \Delta P_1 + \Delta P_2 + \Delta P_T$, where the three terms account for the pressure loss distributed along $L_1$, the pressure loss distributed along $L_2$ and the local pressure loss associated with the T junction (splitting flow, or merging flow). We can express $\Delta P$ as

$$\rho\Delta P = \frac{f_1}{2}\frac{L_1}{D_1^5}\frac{\dot{m}^2}{(\pi/4)^2} + \frac{f_2}{8}\frac{L_2}{D_2^5}\frac{\dot{m}^2}{(\pi/4)^2} + \frac{f_T}{2}\frac{\dot{m}^2}{(\pi/4)^2 D_1^4} \tag{21}$$

where $f_1$ and $f_2$ are friction factors, and $f_T$ is the loss coefficient at the junction. Next, we eliminate $D_1$ between Eqs. (19) and (21). The total mass flow rate is

$$\dot{m}^2 = \frac{\rho\Delta P(V^{5/2}/A^{7/4})}{(\pi/4)^{1/2}R_f} \tag{22}$$

where the overall flow resistance is

$$R_f = \left[\frac{f_1}{2}\tilde{L}_1 + \frac{f_2}{8}\tilde{L}_2\left(\frac{D_1}{D_2}\right)^5\right]\left[\tilde{L}_1 + 2\tilde{L}_2\left(\frac{D_2}{D_1}\right)^2\right]^{5/2} + \frac{f_T}{2}\frac{[\tilde{L}_1 + 2\tilde{L}_2(D_2/D_1)^2]^2}{Sv^{3/2}(\pi/4)^{1/2}} \tag{23}$$

When the total pressure drop, area $A$ and total duct volume $V$ are fixed, maximizing the total mass flow rate is the same as minimizing the flow resistance $R_f$. The lengths of the stem and its branches are related through the constraint $2\tilde{L}_1\tilde{L}_2 = 1$. If all the pipes are round with smooth-walls, and if their respective Reynolds numbers ($Re_{1,2} = U_{1,2}D_{1,2}/\nu$) are in the range $4\times10^3$–$10^5$, then $f_1$ and $f_2$ can be estimated based on the Blasius formula.

$$f_{1,2} = \frac{0.316}{Re_{1,2}^{0.25}} \tag{24}$$

Note further that mass conservation requires $2U_2/U_1 = (D_1/D_2)^2$. The relation between the Reynolds numbers in the stem and the braches is $Re_2 = Re_1 D_1/2D_2$. The Reynolds number in the stem is related to the geometry of the T assembly,

$$Re_1 = \frac{\dot{m}}{\mu A^{1/2}}\frac{Sv^{3/2}}{(\pi/4)^{1/2}}\left[\tilde{L}_1 + 2\tilde{L}_2\left(\frac{D_2}{D_1}\right)^2\right]^{1/2} \tag{25}$$

When the total pressure drop is fixed, the Reynolds number depends on the mass flow rate, the svelteness value and the size of the area. For splitting flow through a standard threaded T junction made of malleable iron Idelchik [17] recommends

$$f_T = 1 + K\left(\frac{U_2}{U_1}\right)^2 \tag{26}$$

with $K \cong 1.5$. For merging flows, the junction loss factor is

$$f_T = \frac{\Delta P}{\frac{1}{2}\rho U_1^2} = 1 + \left(\frac{D_1}{D_2}\right)^2 + 3\left(\frac{D_1}{D_2}\right)^2\left[\left(\frac{Q_2}{Q_1}\right)^2 - \frac{Q_2}{Q_1}\right] \tag{27}$$

where $Q_1$ and $Q_2$ are the volumetric flow rates along $L_1$ and $L_2$. In our case $Q_1 = 2Q_2$, and Eq. (23) becomes

$$f_T = 1 + \frac{1}{4}\left(\frac{D_1}{D_2}\right)^4 \tag{28}$$

showing that the overall flow resistance expression is the same as substituting $K = 1$ in Eq. (26). For both splitting and merging flows, the first term of Eq. (23) accounts for the pressure losses distributed along $L_1$ and $L_2$, and the second term accounts for the local pressure loss at the T junction.

If we assume that the second term is Eq. (23) is negligible, we can minimize the first term with respect to $L_2/L_1$ and $D_2/D_1$, and the optimal configuration with negligible junction losses is

$$\left(\frac{L_2}{L_1}\right)_{\text{opt}} = 0.881 \quad \left(\frac{D_2}{D_1}\right)_{\text{opt}} = 0.754 \tag{29}$$

We combined Eqs. (23)–(28) and minimized the global flow resistance. Fig. 7 shows the optimal diameter ratio, and Fig. 8 the optimal length ratio or the optimal aspect ratio of the area for both flow directions. All curves in Figs. 7 and 8 approach the limit of negligible junction losses, Eq. (29), as $Sv$ increases.

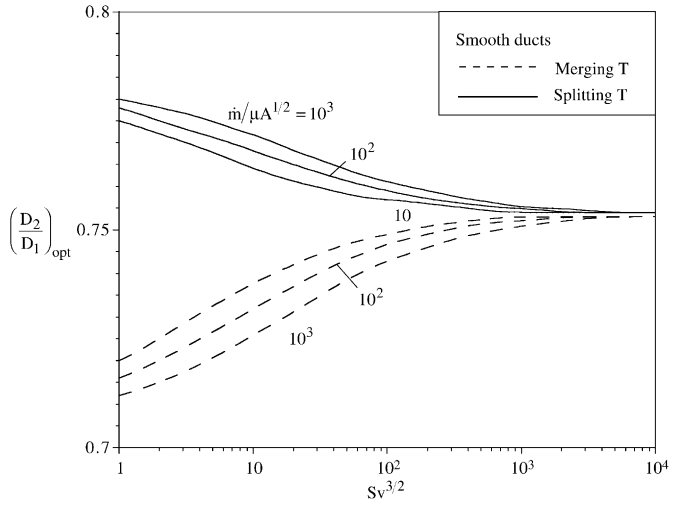


Fig. 7. The optimal diameter ratio for T-shaped constructs of round smooth pipes with turbulent flow.

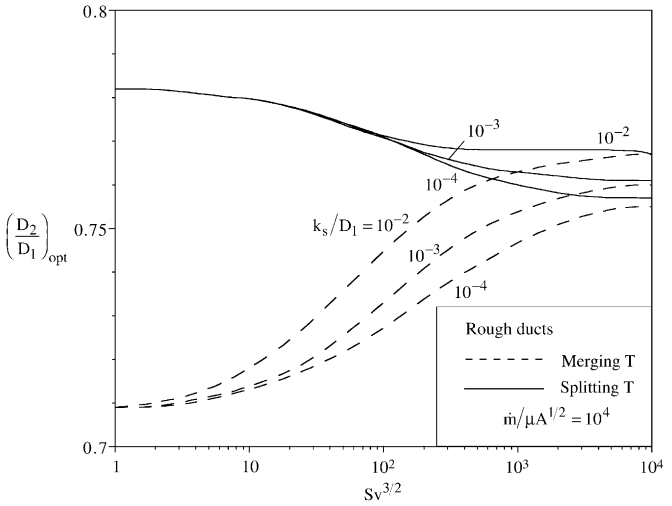


Fig. 9. The optimal diameter ratio for T-shaped constructs of round rough pipes with turbulent flow.

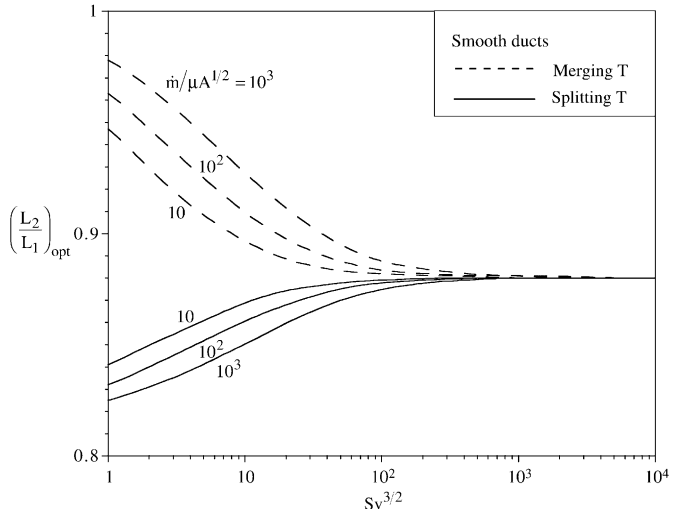


Fig. 8. The optimal external aspect ratio for T-shaped constructs of round smooth pipes with turbulent flow.

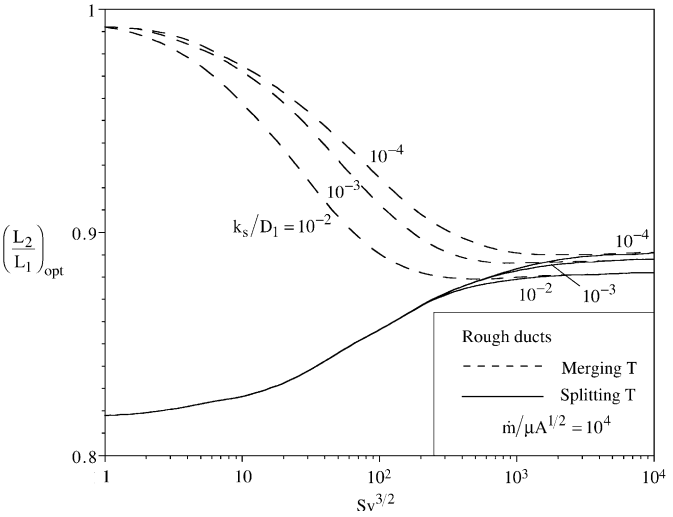


Fig. 10. The optimal external aspect ratio for T-shaped constructs of round rough pipes with turbulent flow.

## 5. Turbulent flow through rough ducts

The effect of wall roughness brings about a complication that is not present in the classical analysis of pressure drop along a duct with rough walls. In the classical calculation (e.g., Moody chart [18]) the roughness of the wall is accounted for in terms of a dimensionless constant, $k_s/D$, where $k_s$ is the height of asperities, and $D$ is the duct hydraulic diameter. In the present work there are two roughness parameters, $k_{s1}/D_1$ and $k_{s2}/D_2$, and both vary because $D_1$ and $D_2$ vary during the optimization of the entire structure. In other words, even though the wall material is specified, the relative roughness of each duct varies during optimization. Miller [19] proposed the following formula for estimating the friction factor for rough pipes,

$$f_i = \frac{0.25}{\left[\log\left(\frac{k_{s,i}/D_i}{3.7} + \frac{5.74}{Re_i^{0.9}}\right)\right]^2} \tag{30}$$

We assumed that the stem and the two branches are made of the same material, such that $k_{s1} = k_{s2} = k_s$. In this case the friction factors for the stem and branches are

$$f_1 = \frac{0.25}{\left[\log\left(\frac{k_s/D_1}{3.7} + \frac{5.74}{Re_1^{0.9}}\right)\right]^2} \tag{31}$$

$$f_2 = \frac{0.25}{\left[\log\left(\frac{(k_s/D_1)(D_1/D_2)}{3.7} + \frac{5.74}{(D_1 Re_1/2D_2)^{0.9}}\right)\right]^2} \tag{32}$$

Next, we replaced Eq. (24) with Eqs. (31) and (32), calculated the friction factors, and repeated the analysis of Section 4 in order to minimize the flow resistance $R_f$. To

investigate the effect of the surface roughness on the optimal configuration, we set $\dot{m}/\mu A^{1/2}$ equal to $10^4$. Figs. 9 and 10 show the effect of the relative roughness on the optimal diameter ratio and the optimal length ratio, respectively. The effect of surface roughness is such that at high $Sv$ the optimal diameter and length ratios are different than the values obtained for the smooth-walls limit in Eq. (29).

## 6. Conclusions

In this paper we conducted a fundamental study of the effect of junction losses on the optimized geometry of tree-shaped flows. The new focus is geometry, not performance. We investigated systematically several classes of flows: laminar through parallel-plates channels, turbulent flow through pipes with smooth-walls, and turbulent flow through pipes with rough walls.

For each class, we showed two things: (i) how junction losses affect the optimized geometry, and (ii) the parametric domain in which it is permissible to neglect junction losses in the optimization of tree architecture. An important conclusion is that the domain (ii) is governed by the svelteness ($Sv$) of the entire structure. The domain in which junction losses have an important effect on the optimized geometry is $Sv^2 < 10$. This is true for both laminar and turbulent flow.

Another important conclusion was revealed by Fig. 2. The links (channels, ducts) of tree-shaped architectures are destined to become less slender as such architectures become finer, more complex. In time, the pursuit of maximum compactness (heat transfer density) leads to structures with smaller (finer) and more numerous details. Less slender ducts mean a smaller $Sv$ value, and a greater effect of junction losses on geometry. This conclusion is particularly important in the design of dendritic microchannels for future heat transfer devices for cooling electronics.

We also explored the relationship (and differences) between the svelteness $Sv$ of the flow system (a global property) and the slenderness of each channel, $L_i/D_i$ (a local property). The two properties are related qualitatively, but are not the same.

In sum, this study makes a statement on the validity of most of the literature on tree-shaped flow architectures, where junction losses are routinely neglected. Now we see that the routine assumption of Poiseuille flow means that the $Sv$ value must be large. Such an assumption must be spelled out in the future. For example, if the tube length $L_i$ scales as $L$, and the tube diameter $D_i$ scales as $V^{1/3}$, then the Poiseuille flow occupies most of the tube length when the tube entrance length $D_i Re_{D_i}$ is much shorter than $L$. This translates into the requirement $L_i/D_i \gg Re_{D_i}$, which means that $Sv$ must be greater than $Re_{D_i}$.

## References


[1] A. Bejan, I. Dincer, S. Lorente, A.F. Miguel, A.H. Reis, Porous and Complex Flow Structures in Modern Technologies, Springer, New York, 2004.

[2] A. Bejan, S. Lorente, La Loi Constructale, L'Harmattan Paris, 2005.

[3] A. Bejan, Constructal-theory network of conducting paths for cooling a heat generating volume, Int. J. Heat Mass Transfer 40 (1997) 799–816, published on 1 November 1996.

[4] L.A.O. Rocha, S. Lorente, A. Bejan, Constructal design for cooling a disc-shaped area by conduction, Int. J. Heat Mass Transfer 45 (2002) 1643–1652.

[5] J. Lewins, Bejan's constructal theory of equal potential distribution, Int. J. Heat Mass Transfer 46 (2003) 1541–1543.

[6] A. Bejan, M.R. Errera, Convective trees of fluid channels for volumetric cooling, Int. J. Heat Mass Transfer 43 (2000) 3105–3118.

[7] D.V. Pence, Reduced pumping power and wall temperature in microchannel heat sinks with fractal-like branching channel networks, Microscale Thermophys. Eng. 6 (2002) 319–330.

[8] A.Y. Alhabi, D.V. Pence, R.N. Callion, Fluid flow through microscale fractal-like branching channel networks, J. Fluids Eng. 125 (2003) 1051–1057.

[9] Y. Chen, P. Cheng, Heat transfer and pressure drop in fractal tree-like microchannel nets, Int. J. Heat Mass Transfer 45 (2002) 2643–2648.

[10] H. Brod, Residence time optimized choice of tube diameters and slit heights in distribution systems for non-Newtonian liquids, J. Non-Newtonian Fluid Mech. 111 (2003) 107–125.

[11] W. Wechsatol, S. Lorente, A. Bejan, Optimal tree-shaped networks for fluid flow in a disc-shaped body, Int. J. Heat Mass Transfer 45 (2002) 4911–4924.

[12] S.M. Senn, D. Poulikakos, Tree network channels as fluid distributors constructing double-staircase polymer electrolyte fuel cells, J. Appl. Phys. 96 (1) (2004) 842–852.

[13] S.M. Senn, D. Poulikakos, Laminar mixing, heat transfer and pressure drop in tree-like microchannel nets and their application for thermal management in polymer electrolyte fuel cells, J. Power Sources 130 (2004) 178–191.

[14] S. Lorente, A. Bejan, Svelteness, freedom to morph, and constructal multi-scale flow structures, Int. J. Thermal Sci. 44 (2005) 1123–1130.

[15] FIDAP Theory Manual, Fluid Dynamics International, Evanston, IL, Revision 8.6, 1998.

[16] M. Aydin, A.F. Miguel, E.D. Aydin, A.H. Reis, Numerical simulation of flow in T channel by boundary element method, in: Proceedings of the First International Exergy, Energy and Environment Symposium, 13–17 July, 2003, Izmir, Turkey, pp. 119–122.

[17] I.E. Idelchik, Handbook of Hydraulic Resistance, second ed., Hemisphere, Washington, DC, 1986.

[18] A. Bejan, Convection Heat Transfer, third ed., Wiley, New York, 2004, p. 387.

[19] R.W. Miller, Flow Measurement Engineering Handbook, third ed., McGraw-Hill, New York, 1996.